Cureus Journal of Engineering

Open Access Original Article

A Novel Setup For Realization of Periodic Arbitrary Patterns Through Interference Lithography

Received 07/24/2025
Review began 10/12/2025
Review ended 12/18/2025
Published 01/14/2026

DOI:
https://doi.org/10.7759/s44388-025-00012-3

Mahdi Kordi [1] , Seyed Mohammad Reza Vaziri [1] , Mojtaba Joodaki [2]

1. Electrical Engineering/Communications Engineering, Ferdowsi University of Mashhad, Mashhad, IRN 2. Computer Science and Engineering/Electrical Engineering, Constructor University, Bremen, DEU

Corresponding author: Mojtaba Joodaki, mjoodaki@constructor.university

Abstract

The two-dimensional (2D) Fourier series expansion technique is a fundamental tool for generating arbitrary 2D patterns in interference lithography. Indeed, this article is 2D extension to our previous work for 1D interference lithography, introduced in our previous paper. In this approach, an inequality on the magnitude of electric field on the surface of photoresist is addressed. Since an analytic solution to this inequality is complicated, we present an estimated solution with two degrees of freedom. Furthermore, an intuitive perspective on the general case of interference lithography is provided, elucidating the relationship between the number of interfering plane waves and the achievable resolution, and showing that a relatively small number (e.g., 9-11) is sufficient to reproduce sub-wavelength features. Finally, a new optical configuration is proposed to enable the practical implementation of our interference lithography approach for generating 2D periodic arbitrary patterns. By combining the proposed formulation and optical configuration, this study demonstrates that interference lithography can be systematically extended to generate almost any arbitrary 2D patterns using a limited number of plane waves.

The capability of the proposed approach in producing complex 2D periodic patterns is demonstrated using two examples. In the first case, a unit cell of 12λ × 12λ containing concentric circular features with widths as small as one wavelength (λ) was successfully reconstructed using 11 plane waves (M = N = 5). In the second example, a 10λ × 10λ pattern composed of a 1.5λ-wide strip, a circular feature of radius 1.5λ, and a ring with inner and outer radii of 2λ and 3.5λ, respectively, was reproduced using only 9 plane waves (M = N = 4). The method can achieve feature sizes down to approximately 150 nm under UV exposure (λ_0 = 365 nm) when 10-15 plane waves are used.

Categories: Electronics Design and VLSI, Nanoelectronics and Quantum Computing, Nanotechnology
Keywords: interference lithography, fourier series expansion, manipulation of plane waves, optical analysis, maskless lithography

Introduction

Although interference lithography can be used in conjunction with masks, it is generally considered a maskless lithography technique. This approach is fast and reduces the additional costs associated with implementing lithography patterns [1-4]. However, the main bottleneck of this method is that it can only produce certain special periodic patterns [5]. Producing nano scale antennas, gratings, metamaterial structures, and rectennas are among the different applications of interference lithography [6,7]. There are some methods for interference of the waves, like using Lloyd's mirror [8], a prism [9], a grating [10] and excitation of plasmons [11]. A frequently used structure to interfere the waves is interference using higher order modes of gratings [12,13]. In [13], interference of two to six waves is reported and a minimum half pitch of 22 nm is achieved at EUV wavelengths (13.5 nm). Albeit, by increasing the number of interfering waves, more variety of patterns can be created but at the cost of decreasing the depth of focus and increasing the complexity of the lithography system. It is worth mentioning that producing the required gratings is a practical challenge, too. Prism is another instrument that provides a mechanism for interference of the waves, which is simple, reliable, and cheap [14-16], but the variety of produced patterns is still limited with this method.

As another kind of interference lithography, interfering of surface and bulk plasmon polaritons have been realized [17-19]. Their main advantage is having higher propagation constant relative to the incident wave that is equivalent to smaller wavelengths for interference lithography and hence, better resolutions. However, controlling the magnitude and phase of the interfered waves is very difficult. Also, all of excited waves have the same propagation constant that limits the variety of obtainable patterns.

By extending our methodology from 1D to 2D patterns, we significantly enhance our previous work [5]. This approach eliminates the main limitation of interference lithography, thus broadening the range of

How to cite this article
Kordi M, Vaziri S, Joodaki M (January 14, 2026) A Novel Setup For Realization of Periodic Arbitrary Patterns Through Interference Lithography. Cureus J Eng 3 : es44388-025-00012-3. DOI https://doi.org/10.7759/s44388-025-00012-3

obtainable patterns through Fourier series expansion (FSE) technique. In this manuscript, creation of 2D periodic arbitrary patterns is discussed, first. Next, the relationship between the proposed method resolution and the number of the interfering waves is investigated in 2D cases. Afterwards, two examples on 2D patterns are considered and then a setup is presented for our proposed lithography method.

It should be noted that in our approach, in principle, any arbitrary pattern can be realized when the number of plane waves is unrestricted. In practice, however, the number of plane waves is finite, which limits the achievable complexity of the patterns. But even with this practical constraint, the proposed method enables the generation of patterns that are significantly more complex than those attainable using existing interference lithography approaches.

Materials And Methods

2D periodic arbitrary patterns

Based on 2D Fourier analysis, any arbitrary electric field distribution which is periodic in *x* and *y* directions, can be expanded as a sum of plane waves as follows:

$$E(x,y,z)=\sum_{m=-M}^{M}\sum_{n=-N}^{N}e^{-jk_{x,m}x}\,e^{-jk_{y,n}y}\,e^{-jk_{z,mn}z}\left[A(k_{x,m},k_{y,n})\,a_x+B(k_{x,m},k_{y,n})\,a_y+C(k_{x,m},k_{y,n})\,a_z\right] \quad (1)$$

where $A(k_{x,m},k_{y,n}),$, $A(k_{x,m},k_{y,n}), B(k_{x,m},k_{y,n})$, and $C(k_{x,m},k_{y,n})$ are the Fourier coefficients related to the amplitudes of electric field components in *x*, *y*, and *z* directions, respectively. By assuming T_x and T_y as the periodicity of the function in *x* and *y* directions, we have $k_{x,m}=2m\pi/T_x, k_{y,n}=2n\pi/T_y$ and

$$k_{z,mn}=\begin{cases}\sqrt{k_0^2-k_{x,m}^2-k_{y,n}^2} & \text{if } k_0^2\geq k_{x,m}^2+k_{y,n}^2\\ -j\sqrt{k_{x,m}^2+k_{y,n}^2-k_0^2} & \text{if } k_0^2< k_{x,m}^2+k_{y,n}^2\end{cases} \quad (2)$$

where k_0 is the free-space wavenumber. Also, this equation satisfies the Helmholtz equation. The corresponding wave vector for each plane wave is obtained from, $\mathbf{k}=k_{x,m}\mathbf{a}_x+k_{y,n}\mathbf{a}_y+k_{z,mn}\mathbf{a}_z$. By placing the photoresist at $z=0$ plane, the electric field on this surface can be calculated from

$$E(x,y,0)=\sum_{m=-M}^{+M}\sum_{n=-N}^{+N}e^{-jk_{x,m}x}\,e^{-jk_{y,n}y}\left[A(k_{x,m},k_{y,n})\,\mathbf{a}_x+B(k_{x,m},k_{y,n})\,\mathbf{a}_y+C(k_{x,m},k_{y,n})\,\mathbf{a}_z\right] \quad (3)$$

The functions $A(k_{x,m},k_{y,n}), B(k_{x,m},k_{y,n})$, and $C(k_{x,m},k_{y,n})$ are related to each other through Maxwell' s equations. With respect to orthogonality of the electric field and the propagation direction of a plane wave, we have

$$\mathbf{E}\cdot\mathbf{k}=0 \quad (4)$$

therefore,

$$E_z=\left(\frac{-k_{x,m}}{k_{z,mn}}\right)E_x+\left(\frac{-k_{y,n}}{k_{z,mn}}\right)E_y \quad (5)$$

The intensity of electric field could be obtained from

$$|E(x,y,0)|^2=|E_x(x,y,0)|^2+|E_y(x,y,0)|^2+|E_z(x,y,0)|^2 \quad (6)$$

Assume E_{th} is the threshold value needed for a positive photoresist to be developed after a specific exposure time. A positive photoresist is used throughout this paper and consequently, the output pattern will correspond to the exposed areas. Hence, the magnitude of electric field has to be greater than this threshold value in the areas that we want them to be developed ("on" areas). In the following, $f(x,y)=1$ corresponds to the "on" regions, while $f(x,y)=0$ represents the darker regions. Therefore, our problem is reduced to solving the following inequality,

$$|E(x,y,0)| = \begin{cases} > E_{\text{th}} & \text{if } f(x,y)=1 \\ < E_{\text{th}} & \text{if } f(x,y)=0 \end{cases} \quad (7)$$

Inequality (7) indicates |E(x,y,0)| should be smaller than E_{th} only in darker areas, in the ideal case. In practice, finding a closed form solution to (7) is very difficult, if not impossible. We suggest a solution as follows:

$$E_x(x,y,0) = \begin{cases} f_1(x,y)\, e^{j\varphi_1(x,y)} & f(x,y)=1 \\ 0 & f(x,y)=0, \end{cases} \quad (8)$$

$$E_x(x,y,0) = \begin{cases} f_2(x,y)\, e^{j\varphi_2(x,y)} & \text{if } f(x,y)=1 \\ 0 & \text{if } f(x,y)=0 \end{cases} \quad (9)$$

and $E_z(x,y,0)$ can be calculated using Equation (5). The functions $f_1(x,y), \varphi_1(x,y), f_2(x,y)$, and $\varphi_2(x,y)$ are the magnitudes and phases of $E_x(x,y)$ and $E_y(x,y)$, respectively. These functions should be chosen such that inequality (7) is satisfied. This inequality have infinite number of exact solutions, if we could have infinite number of plane waves. However, in practice, we can encounter a limited number of waves that may introduce errors, particularly in darker regions. Here, "error" is defined as $[|E(x,y,0)| \quad \text{wherever } f(x,y)=1]$ and $|E(x,y,0)| > E_{th}$ in locations where $[f(x,y)=0]$. Thus, to mitigate these errors, an optimization process appears necessary for determining the functions $f_1(x,y)$ and $f_2(x,y)$. Note that $\varphi_1(x,y)$ and $\varphi_2(x,y)$ affect the magnitude of $|E_z(x,y,0)|$ and consequently, inequality (7); hence, they are two arbitrary real functions which can be helpful in the optimization process. Equations (8) and (9) along with Equation (5) yield to

$$A(k_x,m,k_y,n) = \frac{1}{T_xT_y}\int_{T_x}\int_{T_y} f_1(x,y) \times e^{j\phi_1(x,y)} e^{+jk_xmx} e^{+jk_yny}\, dx\, dy \quad (10)$$

$$B(k_x,m,k_y,n) = \frac{1}{T_xT_y}\int_{T_x}\int_{T_y} f_2(x,y) \times e^{j\phi_2(x,y)} e^{+jk_xmx} e^{+jk_yny}\, dx\, dy \quad (11)$$

$$C(k_{x,m},k_{y,n}) = \left(\frac{-k_{x,m}}{k_{z,mn}}\right) A(k_{x,m},k_{y,n}) + \left(\frac{-k_{y,n}}{k_{z,mn}}\right) B(k_{x,m},k_{y,n}) \quad (12)$$

Interference and resolution

According to Equation (2), two types of plane waves can exist [20], propagating waves with the condition, $[k_0^2 \geq k_{x,m}^2 + k_{y,n}^2]$ and evanescent waves with the condition, $k_0^2 < k_{x,m}^2 + k_{y,n}^2$. In order to reconstruct any arbitrary 2D pattern, all the required plane waves have to be excited, propagating and evanescent waves. However, in practice, we often encounter limitations where we can only generate propagating waves. This is primarily due to the significant challenges and difficulties associated with producing and controlling the specifications of evanescent waves.

Figure *1* shows a wave vector diagram with $k_{x,m} and k_{y,n}$ as its axes. With respect to Equation (2), only the plane waves that their k_x and k_x, lie inside the circle with the radius of k_0 are propagating waves and the others are evanescent. For instance, each cross in Figure *1* is related to a specific pair of *m* and *n* in $k_{x,m} = \frac{2m\pi}{T_x} and k_{y,n} = \frac{2n\pi}{T_y}$. The red crosses within the circle, correspond to propagating waves while yellow crosses located outside the circle, represent the evanescent waves.

As an intuitive insight about the interference lithography, the more values for $T_x/\lambda and T_y/\lambda$, the more propagating waves exist and hence, more complicated patterns could be created with better resolutions but, at the cost of lower depth of focus. As another point, the period of pattern should be greater than the wavelength; because, if either $T_x/\lambda < 1 or T_y/\lambda < 1$, the only propagating term that can participate in interference is the pair of $m = n = 0$.

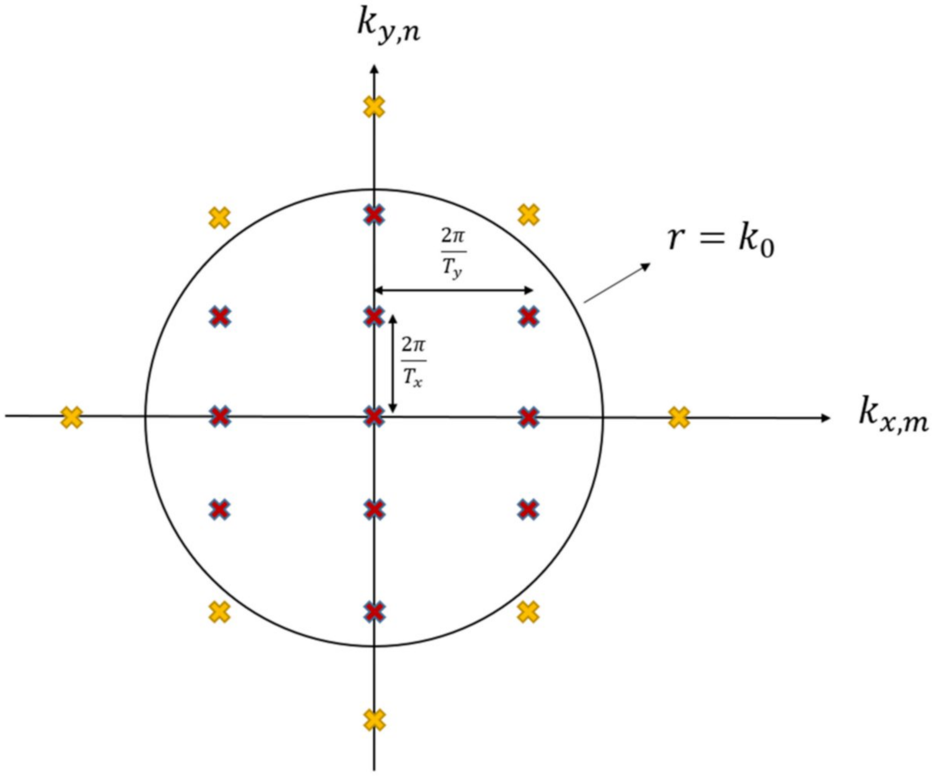

FIGURE 1: The wave vectors of propagating and evanescent waves

The y component of wave vector ($k_{y,n}$) versus its x component ($k_{x,m}$). The circle separates the propagating waves from evanescent waves.

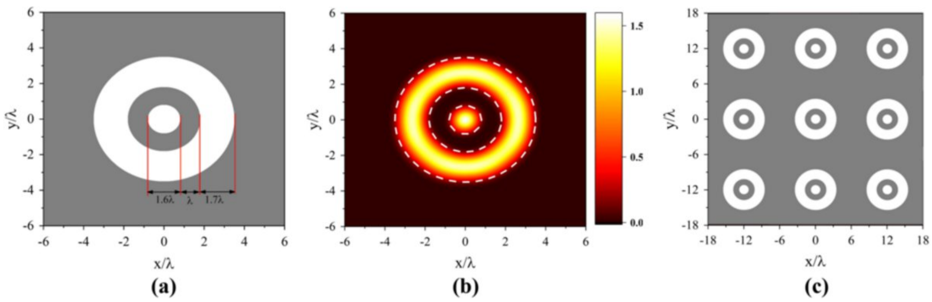

FIGURE 2: The first example

(a) The desired pattern of the first example. (b) The resulted electric field intensity distribution at $z = 0$. (c) a 3×3 array of the pattern shown in (a). In (b), the white dashed lines show the boundaries of the desired pattern. The inner and outer radii of the white ring in (a) are 1.8λ and 3.5λ, respectively, and radius of the inner circle is 0.8λ.

Examples

To investigate the ability of our proposed methodology, two examples are considered in this section. The first example which is shown in Figure 2(a), studies a unit cell with the dimensions of $12\lambda \times 12\lambda$. Note that the possible simplest solution to the inequality (7) is to choose $f_1(x, y)$ and $f_2(x, y)$ as factors multiplied by $f(x, y)$. This factor has to be chosen such that the generated pattern and the ideal one have the maximum similarity. This factor could be controlled by adjusting the intensity of light source or its exposure time. The desired pattern and the parameters for the realization of this example are as follows:

$$f(x,y)=\begin{cases}1 & \text{if } x^2+y^2<(0.8\lambda)^2\\ 1 & \text{if } (1.8\lambda)^2<x^2+y^2<(3.5\lambda)^2\\ 0 & \text{otherwise}\end{cases} \tag{13}$$

$$\begin{cases}M=N=5,\\ f_1(x,y)=f_2(x,y)=1.265\,f(x,y),\\ \varphi_1(x,y)=\varphi_2(x,y)=0,\\ E_{th}=1\end{cases} \tag{14}$$

Figure 2(b) shows the electric field distribution at the surface of photoresist ($z=0$). As can be seen, the inner dark ring (the region between the inner circle and the ring) with the width of λ can be easily distinguished. For a better understanding, an array of 3×3 of the ideal unit cell (Figure 2(a)) is given in Figure 2(c).

The next example is shown in Figure 3(a) that contains one strip, a circle and the donate-shaped ring in its unit cell with the dimensions of $10\lambda\times 10\lambda$. The width of the strip is 1.5λ, inner and outer radii of the ring are 2λ and 3.5λ, respectively, and the radius of circle is 1.5λ. The corresponding intensity distribution of the electric field at $z=0$ is sketched in Figure 3(b) and the corresponding cross section is depicted in Figure 3(c). As can be seen in these figures, an acceptable result is obtained through our proposed method. The desired pattern and the parameters used for these calculations are as follows:

$$f(x,y)=\begin{cases}1, & -4.5\lambda<x<-3\lambda,\\ 1, & (x-\lambda)^2+y^2<(1.5\lambda)^2,\\ 1, & (2\lambda)^2<(x-\lambda)^2<(3.5\lambda)^2,\\ 0, & \text{otherwise}\end{cases} \tag{15}$$

$$\begin{cases}M=N=4\\ f_1(x,y)=\begin{cases}1.12 & \text{if } -4.5\lambda<x<-3\lambda\\ 0 & \text{otherwise}\end{cases}\\ f_2(x,y)=\begin{cases}1 & \text{if } (x-1\lambda)^2+y^2<(1.5\lambda)^2\\ 1 & \text{if } (2\lambda)^2<(x-1\lambda)^2+y^2<(3.5\lambda)^2\\ 0 & \text{otherwise}\end{cases}\\ \varphi_1(x,y)=\varphi_2(x,y)=0\\ E_{th}=0\end{cases} \tag{16}$$

For the sake of simplicity in these examples, $\varphi_1(x,y)$ and $\varphi_2(x,y)$ are assumed to be equal to zero, while optimization of these parameters can lead to better results.

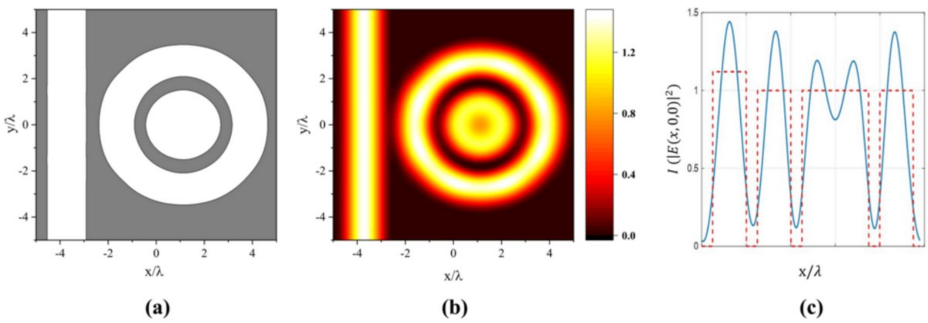

FIGURE 3: The second example

(a) The desired pattern of the second example. (b) The resulted electric field intensity distribution at $z=0$. (c) Cross section of (b) at $y=0$. The inner and outer radii of the white ring in (a) are 2λ and 3.5λ, respectively and radius of the inner circle is 1.5λ. The width of the strip is 1.5λ, too.

Results And Discussion

Realization of the required propagating plane waves

All the derivations presented in the previous sections should be realized using plane wave sources with specific characteristics. In this section, a setup is presented to provide plane waves with specific magnitude, phase, polarization, and propagation direction. Below, we describe our proposed methodology to obtain these objectives. The required waves can be produced using a monochromatic source and a number of beam conditioners equal to the number of Fourier terms.

Tuning of Wave Characterization

Although a polarizer is a component used to change the polarization of a wave, it can be used to control the magnitude of the wave, too. While a linearly-polarized wave collide with a linear polarizer, in the normal direction, we have

$$I_{\text{out}} = I_{\text{in}} \cos^2(\theta) \qquad (17)$$

where I_{out} and I_{in} are output and input intensities, respectively. Also, θ is the angle between the polarization axis of the input wave and the axis of the polarizer. As a result, we propose two polarizers to control the magnitude and polarization of the wave together, as shown in Figure *4*. In this way, the direction of the second polarizer has to be set along the required polarization (θ_2 in Figure *4*) and the direction of the first one (θ_1 in Figure *4*) should be derived with respect to Equations (18) and (19). Note that the transmission coefficient of the electric field (T) and θ_2 are the desired known values that have already been calculated from FSE derivations.

$$I_2 = I_1 cos^2(\theta_2 - \theta_1) = I_0 cos^2(\theta_1) cos^2(\theta_2 - \theta_1), \qquad (18)$$

$$T = \sqrt{\frac{I_2}{I_0}} = \cos(\theta_1)\cos(\theta_2 - \theta_1) \qquad (19)$$

The phase of the plane waves can be controlled by changing the electrical paths of the waves, passing through the beam conditioners. Parameters l_1, l_2, l_3, and l_4 are the distances from the source to the mirror, from the mirror to the first polarizer, from the first polarizer to the second polarizer and from the second polarizer to the photoresist, respectively, and are depicted in Figure *5*(b). The distance $l_1 + l_2$ changes, if the mirror is displaced in the z direction in Figure *5*(b). More details are described in [5]. On the other hand, the propagation directions of the waves can be controlled by adjusting the orientation of the mirrors.

The Proposed Setup

Based on the previous sections, the general schematic of the proposed setup is sketched in Figure *5*(a) and the details of a beam conditioner are shown in Figure *5*(b), which consists of two polarizers and a mirror. The displacement of this mirror in the *z* direction can alter the electrical path, thereby affecting the phase of the corresponding plane wave. Therefore, by implementing the setup depicted in Figure *5*(b), a plane wave with arbitrary magnitude, phase, polarization, and propagation direction can be produced. It should be noted that since adjusting one specification can affect and deteriorate the others, there should be a hierarchy in tuning the desired parameters. The following sequence should be used in the tuning process: propagation direction, polarization, magnitude, and phase. In this way, none of the previously adjusted characteristics are affected.

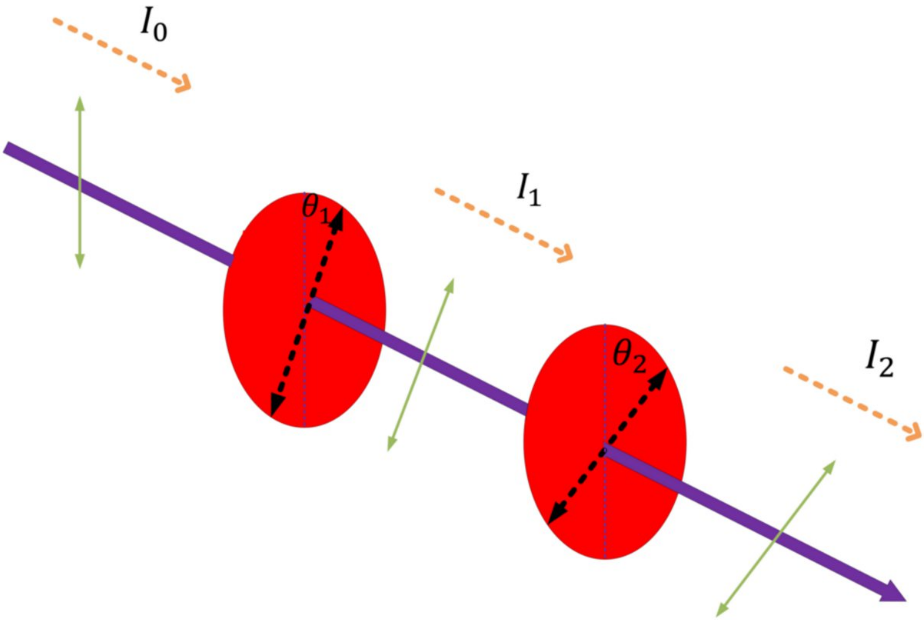

FIGURE 4: Travelling of a wave through two polarizers

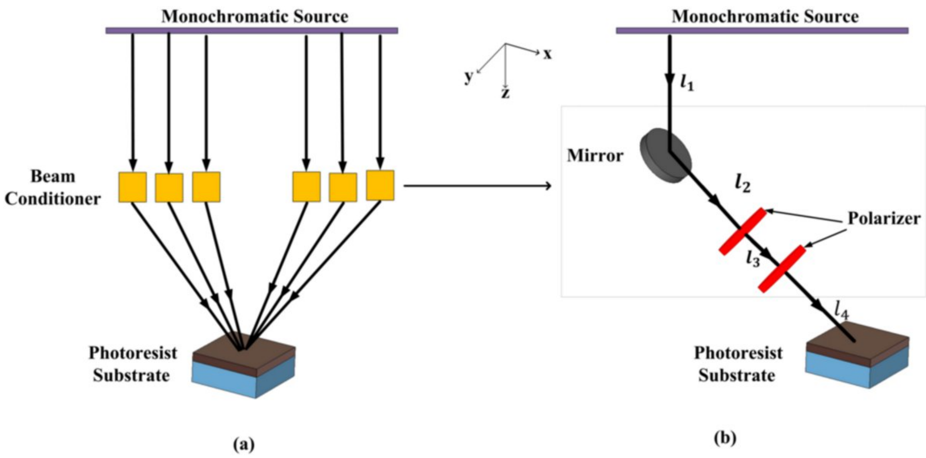

FIGURE 5: (a) General schematic of the proposed system. (b) A beam conditioner in more details

Discussions

In principle, our method is theoretically capable of resolving any periodic arbitrary pattern; however, in practice, the setup complexity increases with the number of the required plane waves. Fortunately, for many applications employing only 10 to 15 plane waves is sufficient to form the desired pattern. The key advantage of our proposed setup, compared to other interference lithography setups, is its tunability and the variety of outputs that it can produce. Theoretically, the proposed system is wavelength-independent, and as long as the components, including mirrors and polarizers, remain functional, the system's performance is maintained. However, in practice, standard mirrors and polarizers suitable for optical wavelengths and the UV range are not applicable at EUV wavelengths. Since the resolution of interference lithography is approximately half the wavelength, the expected minimum feature size of the proposed system cannot go beyond 150 nm under UV exposure.

To create a variety of patterns, we need different propagating waves, therefore each unit cell period of the array (T_x and T_y) should be several times the wavelength. For example, if $\lambda_0 = 365nm$, achieving 15 propagating modes requires T_x and T_y to be at least $750\ nm$ and the expected minimum feature size could be around $150\ nm$. Using 10 to 15 plane waves, our method can generate simple structures such as circles, rings, and rectangles, as well as combinations of these shapes. For applications like meta-surfaces and array nano-antennas, our proposed setup can be very effective. Of course, it should be noted that we are still in the early stages of this research and there is a long way to practical realization of this method. As has been seen in many similar cases, the practical implementation of such relatively complex systems requires a much wider and longer theoretical and practical research.

A major advantage of interference lithography is the ability to pattern large areas with a single illumination shot. In industrial production lines, large-scale masks are cost-effective due to the high product volumes. However, for non-commercial products, producing large-area masks is very costly. Therefore, for laboratory and low-volume applications, when an arbitrary pattern is needed, our proposed setup is highly beneficial. Typically, resolving patterns requires multiple lithography steps, and our method can serve as one of these, helping to reduce overall costs.

Conclusions

In order to expand and complete the previous idea in our previous paper, we developed an approach to produce 2D periodic arbitrary patterns utilizing interference lithography. For this purpose, an inequality on the magnitude of the electric field is obtained, and an estimated solution is presented for it. This solution has two degrees of freedom for each component, E_x and E_y (Equations (8) and (9)), which can help to reduce the estimation error and, in some cases, the number of required Fourier terms. Hence, optimization of $f_1(x, y)$ and $f_2(x, y)$ could be an essential step in the future development of our method. Furthermore, a new lithography setup is presented to implement our required plane waves. This system has two polarizers to control the magnitude and polarization of the waves and also a mirror for tuning the required propagation direction and phase. The good controllability of a polarizer makes it a good candidate to adjust the magnitude of a plane wave with ultra-short wavelengths, but at the cost of some extra losses in the system.

It is worth mentioning that a lens system is usually used in conventional photolithography systems to minimize the size of the desired patterns by using higher spatial frequencies. However, in our lithography setup, there is no need for a complicated objective lens system because any spatial frequency, or equivalently any propagation direction, can be produced by adjusting the orientation of the corresponding mirror.

Quantitative analysis of the presented examples confirms that the proposed interference lithography setup can reconstruct arbitrary periodic patterns with high fidelity using a limited number of plane waves (typically 10-15). For instance, a 12λ × 12λ unit cell pattern with subwavelength features was obtained using 11 plane waves, while a 10λ × 10λ composite pattern was achieved with 9 waves. For practical UV lithography (λ0 = 365 nm), these correspond to minimum achievable feature sizes of around 150 nm and unit cell periods on the order of 750 nm, highlighting the system’s potential for high-resolution patterning without the need for complex lens assemblies.

Additional Information

Author Contributions

All authors have reviewed the final version to be published and agreed to be accountable for all aspects of the work.

Concept and design: Mojtaba Joodaki, Mahdi Kordi

Critical review of the manuscript for important intellectual content: Mojtaba Joodaki, Mahdi Kordi, Seyed Mohammad Reza Vaziri

Supervision: Mojtaba Joodaki

Acquisition, analysis, or interpretation of data: Mahdi Kordi, Seyed Mohammad Reza Vaziri

Drafting of the manuscript: Mahdi Kordi

Disclosures

Human subjects: All authors have confirmed that this study did not involve human participants or tissue. **Animal subjects:** All authors have confirmed that this study did not involve animal subjects or tissue. **Conflicts of interest:** In compliance with the ICMJE uniform disclosure form, all authors declare the following: **Payment/services info:** All authors have declared that no financial support was received from any organization for the submitted work. **Financial relationships:** All authors have declared that they have no financial relationships at present or within the previous three years with any organizations that might have an interest in the submitted work. **Other relationships:** All authors have declared that there are no other relationships or activities that could appear to have influenced the submitted work.

References

1. Ma YW, Park JH, Lee SJ, Lee J, Cho S, Shin BS: Fabrication system for large-area seamless nanopatterned cylinder mold using the spiral laser interference exposure method. International Journal of Precision Engineering and Manufacturing-Green Technology. 2023, 10:1-7. 10.1007/s40684-022-00423-1
2. Singhal G, Dewanjee S, Bae G, et al.: Interference lithography-based fabrication of 3D metallic mesostructures on reflective substrates using electrodeposition-compatible anti-reflection coatings for power electronics cooling. Advanced Electronic Materials. 2024, 10:2300827. 10.1002/aelm.202300827
3. Lu T, Deng F, Wei Y, Zeng Z, Li X: Single-cycle contact-interference hybrid lithography for scalable fabrication of arrayed quadrant micro-polarizer structures. International Journal of Extreme Manufacturing. 2025, 8:025102. 10.1088/2631-7990/ae23a0
4. Jiang Z, Zhang X, He W, Jiang K, Wang L: Optimized fabrication of subwavelength slanted gratings via laser interference lithography and faraday cage-assisted etching. Microelectronic Engineering. 2025, 298:112323. 10.1016/j.mee.2025.112323
5. Kordi M, Vaziri SMR, Armin F, Joodaki M: An approach for one dimensional periodic arbitrary lithography based on Fourier series. Engineering Science and Technology, an International Journal. 2021, 24:343-47. 10.1016/j.jestch.2020.08.014
6. Bagheri S, Weber K, Gissibl T, Weiss T, Neubrech F, Giessen H: Fabrication of square-centimeter plasmonic nanoantenna arrays by femtosecond direct laser writing lithography: effects of collective excitations on SEIRA enhancement. ACS Photonics. 2015, 2:779-86. 10.1021/acsphotonics.5b00141
7. Seo JH, Park JH, Kim Sl, Park BJ, Ma Z, Choi J, Ju BK: Nanopatterning by laser interference lithography: applications to optical devices. Journal of Nanoscience and Nanotechnology. 2014, 14:1521-532. 10.1166/jnn.2014.9199
8. Bagal A, Chang CH: Fabrication of subwavelength periodic nanostructures using liquid immersion Lloyd's mirror interference lithography. Optics Letters. 2013, 38:2531-534. 10.1364/ol.38.002531
9. de Boor J, Kim DS, Schmidt V: Sub-50 nm patterning by immersion interference lithography using a Littrow prism as a Lloyd's interferometer. Optics Letters. 2010, 35:3450-452. 10.1364/ol.35.003450
10. Solak HH, David C, Gobrecht J, Golovkina V, Cerrina F, Kim SO, Nealey PF: Sub-50 nm period patterns with EUV interference lithography. Microelectronic Engineering. 2003, 67-68:56-62. 10.1016/s0167-9317(03)00059-5
11. Sreekanth KV, Murukeshan VM: Large-area maskless surface plasmon interference for one- and two-dimensional periodic nanoscale feature patterning. Journal of the Optical Society of America A. 2009, 27:95-99. 10.1364/josaa.27.000095
12. Mojarad N, Fan D, Gobrecht J, Ekinci Y: Broadband interference lithography at extreme ultraviolet and soft x-ray wavelengths. Optics Letters. 2014, 39:2286-289. 10.1364/ol.39.002286
13. Mojarad N, Fan D, Gobrecht J, Ekinci Y: Interference lithography at EUV and soft X-ray wavelengths: Principles, methods, and applications. Microelectronic Engineering. 2015, 143:55-63. 10.1016/j.mee.2015.03.047
14. Huang YJ, Chang TL, Chou HP, Lin CH: A novel fabrication method for forming inclined groove-based microstructures using optical elements. Japanese Journal of Applied Physics. 2008, 47:5287-290. 10.1143/jjap.47.5287
15. Jiang G, Baig S, Wang MR: Prism-assisted inclined UV lithography for 3D microstructure fabrication. Journal of Micromechanics and Microengineering. 2012, 22:085022. 10.1088/0960-1317/22/8/085022
16. Takahashi H, Heo YJ, Shimoyama I: Scalable fabrication of PEGDA microneedles using UV exposure via a rotating prism. Journal of Microelectromechanical Systems. 2017, 26:990-92. 10.1109/jmems.2017.2740177
17. Dong J, Liu J, Liu P, et al.: Surface plasmon interference lithography with a surface relief metal grating. Optics Communications. 2013, 288:122-26. 10.1016/j.optcom.2012.09.072
18. Wang J, Wang Y, Sun L, et al.: Surface plasmon polaritons maskless lithography of metal-dielectric multilayers with tunable resolution. Optik. 2014, 125:6158-161. 10.1016/j.ijleo.2014.06.120
19. Liu H, Kong W, Liu K, et al.: Deep subwavelength interference lithography with tunable pattern period based on bulk plasmon polaritons. Optics Express. 2017, 25:20511-521. 10.1364/oe.25.020511
20. Pendry JB: Negative refraction makes a perfect lens. Physical Review Letters. 2000, 85:3966-969. 10.1103/physrevlett.85.3966